Proceedings of the 2018 IEEE
International Conference on Robotics and Biomimetics
December 12-15, 2018, Kuala Lumpur, Malaysia

Kinematic Optimization of a Continuum Surgical Manipulator

Shu'an Zhang, Yuyang Chen, Qi Li, Bin Zhao, and Kai Xu, *Member, IEEE*

***Abstract*— Researches on robotically-assisted MIS (Minimally Invasive Surgery) thrived in the past decades due to improved postoperative outcomes. A majority of the existing developments followed a similar approach that a manipulator maneuvers a stick-like surgical tool for intra-abdominal surgical tasks. The surgical tool is usually equipped with a wrist for distal dexterity, while the manipulator, holding the surgical tool, is required to realize RCM (Remote Center of Motion) movements in order to prevent the surgical tool from tearing a patient's abdominal wall. On the other hand, a continuum surgical manipulator is potentially able to realize all the intra-abdominal movements without involving an RCM motion. This paper presents the kinematic optimization of such a continuum surgical manipulator. Considerations on the topology, kinematics modeling and optimizations are elaborated. An actual continuum surgical manipulator was constructed according to the optimization results and was demonstrated to be capable to accomplish a few representative desired tasks.**

I. Introduction

Excellent motion accuracy and dexterity of a surgical robotic system can extend surgeons' intervention capabilities and provided enhanced treatment outcomes. Perspectives of robotic assistance in MIS (Minimally Invasive Surgery) have attracted tremendous attentions in the past decades. [1].

However, a majority of the existing designs of the surgical manipulators in robotically-assisted MIS followed a similar approach [2-6]: a manipulator maneuvers a stick-like surgical tool for intra-abdominal surgical tasks. The surgical tool is usually equipped with a wrist for distal dexterity, while the manipulator, holding the surgical tool, is required to realize RCM (Remote Center of Motion) movements in order to prevent the surgical tool from tearing a patient's abdominal wall.

Continuum manipulators are structurally simple and it is relatively easy to realize multiple DoFs (Degrees of Freedom) via serially stacking a few bending segments while keeping the actuators proximally placed. This feature has inspired many applications of continuum manipulators in healthcare practices or surgical robotic systems [7]. As a continuum surgical manipulator is capable to realize multi-DoF movements at its bending segments shown in Fig. 1, it can potentially achieve all the intra-abdominal movements without involving an RCM motion. Then such a strategy would greatly reduce the design complexity of the existing approach where a stick-like surgical tool is used together with an external manipulator.

Such implementations of continuum surgical manipulators have been explored. For example, quite a few multi-DoF continuum manipulators have been incorporated in several surgical robotic systems without using RCM mechanisms [8-12].

Topologies and dimensions of these continuum surgical manipulators should be optimized for improved intra-abdominal kinematic performances. Such optimizations have only been attempted by the studies in [13, 14]. However, as elaborated in Section II, it was found that the configuration potentially with the best kinematic performance from [14], which was used in [10], is not truly kinematically superior if the constraints from the actual construction were considered.

For the aforementioned reasons, this paper proposes a rigid-continuum-hybrid topology of a continuum surgical manipulator. More importantly, dimension synthesis was conducted based on an optimization on its kinematic performance. A preliminary experimental evaluation with the dimension-optimized manipulator was carried out to indicate the effectiveness of the proposed manipulator configuration.

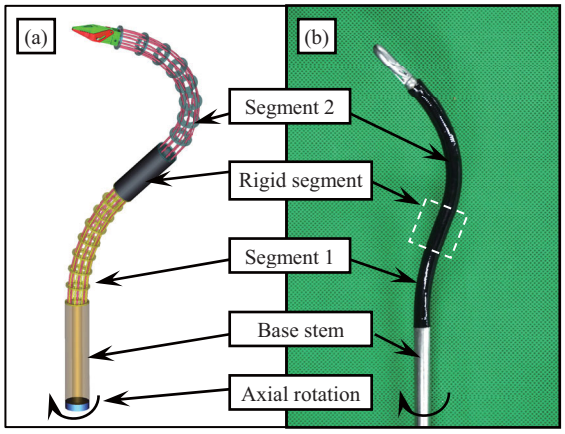

Figure 1. The proposed continuum surgical manipulator: (a) the structural topology, and (b) the constructed manipulator

This paper is organized as follows. Section II presents the considerations for the proposal of the rigid-continuum-hybrid surgical manipulator. Kinematics of the proposed continuum surgical manipulator is derived for the optimization to determine the manipulator's structural dimensions based on a formulation of the kinematic performance in Section III. Construction and preliminary validation of the proposed surgical manipulator with optimized structural parameters are

*This work was supported in part by the National Natural Science Foundation of China (Grant No. 51722507, Grant No. 51435010 and Grant No. 91648103), and in part by the National Key R&D Program of China (Grant No. 2017YFC0110800).

Shu'an Zhang, Yuyang Chen and Bin Zhao are with the RII Lab (Lab of Robotics Innovation and Intervention), UM-SJTU Joint Institute, Shanghai Jiao Tong University, Shanghai, China (emails: jimmyonthego@sjtu.edu.cn, supandoria@sjtu.edu.cn and zhaobin2014@sjtu.edu.cn).

Qi Li and Kai Xu are with the School of Mechanical Engineering, Shanghai Jiao Tong University, Shanghai, China (emails: liqi362202@sjtu.edu.cn and k.xu@sjtu.edu.cn; corresponding author: K. Xu).

978-1-7281-0377-8/18/$31.00 © 2018 IEEE

elaborated in Section IV, while the conclusion and future works are summarized in Section V.

II. Topology Considerations

A surgical manipulator should preferably possess 6 DoFs in order to achieve desired orientations and positions within its intra-abdominal workspace. Most of the existing stick-like surgical tools that are manipulated by an external manipulator have 4 DoFs: panning, tilting, translation and rotation along the tool's axis. The surgical tool hence often possesses a 2-DoF wrist to achieve 6-DoF movements.

On the other hand, 6 DoFs are usually realized differently in continuum surgical manipulators. For example, a continuum manipulator implemented in [15] shown in Fig. 2(a) has three serially stacked inextensible segments. Each segment has two bending DoFs. A rotary wrist is incorporated at the distal end to enhance the orientation reachability. The manipulators implemented in the IREP robot [8] and the SURS robot [10] in Fig. 2(b) and Fig. 2(c) have two 2-DoF inextensible segments stacked on top of a planar translation module and 2 serially stacked extensible 3-DoF segments, respectively. Each 3-DoF segment in Fig. 2(c) has two bending DoFs and one extension DoF.

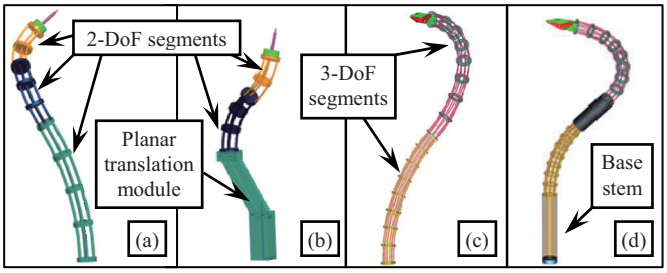

Figure 2. 6-DoF continuum surgical manipulator: (a) 3-segment one, (b) the IREP structure, (c) 2-segment one, and (d) the proposed topology.

As discussed in [14], the manipulator topology in Fig. 2(c) has the best kinematic performance among the ones in Fig. 2(a to c). In that study, the kinematic performance is defined as the capability of orienting the surgical end effector within a predefined functional volume.

The superior kinematic performance of the manipulator in Fig. 2(c) is primarily enabled by the segment extensions. However, the extension capability is often limited by actual implementations: in situations where the continuum surgical manipulator is wrapped by an elastic cover, as shown in Fig. 1(b), the structural extension will be indeed quite small. The fact that the covering is sometimes really necessary to ensure safety (e.g., bio-compatibility) and insertion smoothness makes the topology in Fig. 2(c) much less useful. What's more, extending the segment would reduce the segment's stiffness. It is highly undesired for a surgical manipulator to have inconsistent stiffness across its workspace.

This paper hence proposes an alternative topology for continuum surgical manipulator. The proposed design has 6 DoFs as shown in Fig 2(d): two 2-DoF inextensible segments connected by a rigid straight one are stacked on a straight base stem that can be rotated and translated.

In the proposed topology, the bending segments are made short for relatively high stiffness. The size of the workspace is expanded by the connecting rigid segment. The feeding motion of the base stem also increases the workspace's size. Rotation of the distal surgical end effector will be realized by the synchronized changes in the bending directions of the two bending segments and the rotation of the base stem.

III. Kinematics and Optimization

Nomenclature of the proposed manipulator topology is defined for the modeling and optimization.

The kinematics model is based on the circular bending assumption that provides a simplified yet accurate description of the continuum segments [16, 17]. The kinematics of the t^{th} segment, which can be referred to [10], is briefly summarized in Section III.B. Kinematics of the entire manipulator is derived in Section III.C, while the structural optimization is reported in Section III.D.

A. Nomenclature

Nomenclature of the continuum surgical manipulator is established as in Table I. And the coordinates of the t^{th} segment are detailed as follows.

- The Base Ring Coordinate System (BRS) $\{tb\}=[\hat{\mathbf{x}}_{tb} \quad \hat{\mathbf{y}}_{tb} \quad \hat{\mathbf{z}}_{tb}]^T$ is attached to the base ring of the t^{th} segment, with the XY plane coinciding with the base ring and the X axis passing through the first backbone.
- Bending Plane Coordinate System 1 (BPS1) $\{t1\}=[\hat{\mathbf{x}}_{t1} \quad \hat{\mathbf{y}}_{t1} \quad \hat{\mathbf{z}}_{t1}]^T$ has its origin coincide with that of the BDS of the t^{th} segment and its XY plane coincide with the bending plane of the t^{th} segment.
- Bending Plane Coordinate System 2 (BPS2) $\{t2\}=[\hat{\mathbf{x}}_{t2} \quad \hat{\mathbf{y}}_{t2} \quad \hat{\mathbf{z}}_{t2}]^T$ has its origin located at the center of the end ring of the t^{th} segment and its XY plane aligned with the bending plane of the t^{th} segment.
- End Ring Coordinate System (ERS) $\{te\}=[\hat{\mathbf{x}}_{te} \quad \hat{\mathbf{y}}_{te} \quad \hat{\mathbf{z}}_{te}]^T$ is attached on the end ring of the t^{th} segment, with the XY plane coinciding with the end ring and its X axis passing through the first backbone.

The numbering of the segments is defined in Fig. 3.

Other coordinate systems definitions for the continuum surgical manipulator are shown in Fig. 3(b) and detailed as follows.

- World coordinate system (WS) $\{w\}=[\hat{\mathbf{x}}_w \quad \hat{\mathbf{y}}_w \quad \hat{\mathbf{z}}_w]^T$ is attached to the abdominal incision with its Z axis aligned with the base stem.
- Stem Coordinate System (SS) $\{s\}=[\hat{\mathbf{x}}_s \quad \hat{\mathbf{y}}_s \quad \hat{\mathbf{z}}_s]^T$ is defined to stand for the rotation of the base stem. The angle φ parameterizes the rotation from $\hat{\mathbf{x}}_w$ to $\hat{\mathbf{x}}_s$ along $\hat{\mathbf{z}}_w$.

Note that the origin of $\{s\}$ always coincides with the origin of $\{w\}$. $\hat{\mathbf{z}}_s = \hat{\mathbf{z}}_w$ always holds.

$\{1b\}$ is obtained from $\{s\}$ by a translation of d along $\hat{\mathbf{z}}_s$.

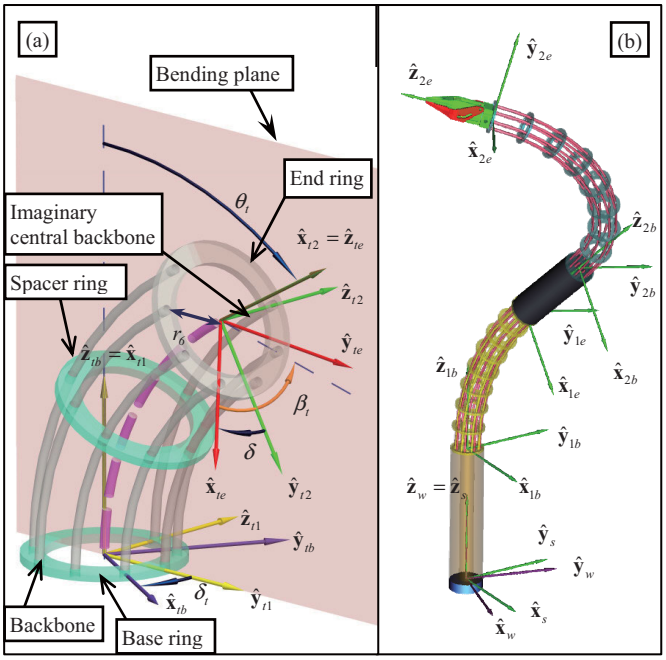

Figure 3. Coordinates and nomenclature: (a) the t^{th} segment, (b) the entire surgical manipulator.

TABLE I. THE NOMENCLATURE USED IN THIS PAPER

Symbol	Definition
t	Index of the segments.
β_t	Division angle of the backbones in the t^{th} segment.
L_t	Length of the imaginary central backbone of the t^{th} segment.
θ_t	The angle indicating the rotation from $\hat{\mathbf{x}}_{t1}$ to $\hat{\mathbf{x}}_{t2}$ about $\hat{\mathbf{z}}_{t1}$.
δ_t	The angle from the bending plane to $\hat{\mathbf{x}}_{tb}$ in the t^{th} segment.
φ	Axial rotation angle of the base stem.
d	Feeding length of the base stem.
$\boldsymbol{\psi}_t$	$\boldsymbol{\psi}_t = [\theta_t \quad \delta_t]^T$ is the configuration vector for the t^{th} segment.
$\boldsymbol{\psi}_s$	$\boldsymbol{\psi}_s = [\varphi \quad d]^T$ is the configuration vector for the base stem.
$\boldsymbol{\psi}$	$\boldsymbol{\psi} = [\boldsymbol{\psi}_s^T \quad \boldsymbol{\psi}_1^T \quad \boldsymbol{\psi}_2^T]^T$ is the configuration vector for the continuum manipulator.
${}^a\mathbf{R}_b$	Coordinate transformation matrix from frame $\{b\}$ to frame $\{a\}$.
${}^a\mathbf{p}_b$	Position vector from the origin of the frame $\{a\}$ to the origin of the frame $\{b\}$ in frame $\{a\}$.
$\mathbf{J}_{tv}, \mathbf{J}_{t\omega}$	Jacobian matrices of linear and angular velocities of the t^{th} segment. $\mathbf{v}_t = \mathbf{J}_{tv}\dot{\boldsymbol{\psi}}_t$ and $\boldsymbol{\omega}_t = \mathbf{J}_{t\omega}\dot{\boldsymbol{\psi}}_t$.

B. Kinematics of the t^{th} Segment

The constant curvature bending assumption is widely used in modeling continuum mechanisms and manipulators, due to its theoretically and experimentally verified validity [10, 16].

The kinematics for the t^{th} continuum segment is summarized as follows.

Center of the end ring of the t^{th} segment is as follows.

$$ {}^{tb}\mathbf{p}_{te} = \frac{L_t}{\theta_t}\begin{bmatrix} \cos\delta_t(1-\cos\theta_t) \\ \sin\delta_t(\cos\theta_t - 1) \\ \sin\theta_t \end{bmatrix} \tag{1} $$

Where ${}^{tb}\mathbf{p}_{te} = [0 \quad 0 \quad L_t]^T$ when $\theta_t \to 0$.

The coordinate transformation matrix ${}^{tb}\mathbf{R}_{te}$ relates $\{te\}$ and $\{tb\}$ as in (2).

$$ {}^{tb}\mathbf{R}_{te} = {}^{tb}\mathbf{R}_{t1}\,{}^{t1}\mathbf{R}_{t2}\,{}^{t2}\mathbf{R}_{te} \tag{2} $$

Where

$$ {}^{tb}\mathbf{R}_{t1} = \begin{bmatrix} 0 & \cos\delta_t & \sin\delta_t \\ 0 & -\sin\delta_t & \cos\delta_t \\ 1 & 0 & 0 \end{bmatrix}, \quad {}^{t1}\mathbf{R}_{t2} = \begin{bmatrix} \cos\theta_t & -\sin\theta_t & 0 \\ \sin\theta_t & \cos\theta_t & 0 \\ 1 & 0 & 0 \end{bmatrix}, $$

and ${}^{t2}\mathbf{R}_{te} = \begin{bmatrix} 0 & 0 & 1 \\ \cos\delta_t & -\sin\delta_t & 0 \\ \sin\delta_t & \cos\delta_t & 0 \end{bmatrix}$.

The instantaneous kinematics for the t^{th} segment is given below.

$$ \dot{\mathbf{x}}_t = \begin{bmatrix} \mathbf{v}_t \\ \boldsymbol{\omega}_t \end{bmatrix} = \mathbf{J}\dot{\boldsymbol{\psi}} = \begin{bmatrix} \mathbf{J}_{tv} \\ \mathbf{J}_{t\omega} \end{bmatrix}\begin{bmatrix} \dot{\theta}_t \\ \dot{\delta}_t \end{bmatrix} \tag{3} $$

Where

$$ \mathbf{J}_{tv} = L_t\begin{bmatrix} \cos\delta_t\left(\frac{\sin\theta_t}{\theta_t} + \frac{(\cos\theta_t - 1)}{\theta_t^2}\right) & \frac{\sin\delta_t(\cos\theta_t - 1)}{\theta_t} \\ \sin\delta_t\left(\frac{(1-\cos\theta_t)}{\theta_t^2} - \frac{\sin\theta_t}{\theta_t}\right) & \frac{\cos\delta_t(\cos\theta_t - 1)}{\theta_t} \\ \frac{\cos\theta_t}{\theta_t} - \frac{\sin\theta_t}{\theta_t^2} & 0 \end{bmatrix} \tag{4} $$

$$ \mathbf{J}_{t\omega} = \begin{bmatrix} \sin\delta_t & \cos\delta_t\sin\theta_t \\ \cos\delta_t & -\sin\delta_t\sin\theta_t \\ 0 & \cos\theta_t - 1 \end{bmatrix} \tag{5} $$

C. Kinematics of the Manipulator

The derived kinematics for the manipulator is expressed in the world coordinate system. The kinematics between the coordinate systems is described below, referring to Fig. 3(b).

- The base stem of the surgical tool can be rotated and fed along $\hat{\mathbf{z}}_w$. $\{s\}$ is obtained from $\{w\}$ by a rotation of φ about $\hat{\mathbf{z}}_w$.
- The continuum segment 1 is stacked on the distal end of the base stem. The attachment of the coordinate systems ($\{1b\}$, $\{t1\}$, $\{t2\}$ and $\{1e\}$ should refer to Section III.A. $\{1b\}$ is translated from $\{s\}$ by a distance of d along $\hat{\mathbf{z}}_s$, $d \in [0, L_0]$. Thus the feeding motion of the base stem is parameterized by d.

- The continuum segment 2 is connected to the segment 1 with a rigid segment (straight) in between. The coordinate systems ($\{2b\}$ and $\{2e\}$) are attached to the continuum segment 2. $\{2b\}$ is obtained from $\{1e\}$ by a translation of L_n along $\hat{\mathbf{z}}_{1e}$. L_n is the length of the rigid segment between the two flexible segments.

The configuration vector $\boldsymbol{\psi} = \begin{bmatrix} \boldsymbol{\psi}_s^T & \boldsymbol{\psi}_1^T & \boldsymbol{\psi}_2^T \end{bmatrix}^T$ parameterizes the kinematics of the continuum manipulator. The tip position of the continuum manipulator is derived as follows.

$$ {}^{w}\mathbf{p}_t = {}^{w}\mathbf{R}_s({}^{s}\mathbf{p}_{1b} + {}^{s}\mathbf{R}_{1b}\,{}^{1b}\mathbf{p}_{1e} + {}^{1b}\mathbf{R}_{1e}({}^{1e}\mathbf{p}_{2b} + {}^{1e}\mathbf{R}_{2b}\,{}^{2b}\mathbf{p}_{2e})) \quad (6) $$

Note that ${}^{s}\mathbf{R}_{1b}$ and ${}^{1e}\mathbf{R}_{2b}$ are identity matrices due to the structure design. The instantaneous kinematics for the manipulator is derived accordingly. The twist of the end effector of the continuum manipulator is as follows.

$$ \dot{\mathbf{x}} = \mathbf{J}\dot{\boldsymbol{\psi}} \quad (7) $$

$$ \mathbf{J} = \begin{bmatrix} \mathbf{W}_1 & {}^{w}\mathbf{R}_{1b}\mathbf{W}_2 & {}^{w}\mathbf{R}_{2b}\mathbf{W}_3 \\ \mathbf{J}_{s\omega} & {}^{w}\mathbf{R}_{1b}\mathbf{J}_{1\omega} & {}^{w}\mathbf{R}_{2b}\mathbf{J}_{2\omega} \end{bmatrix} \quad (8) $$

Where

$$ \mathbf{W}_1 = -\left[{}^{w}\mathbf{p}_{2e}^{1b} \times \right] \cdot \mathbf{J}_{s\omega} + \mathbf{J}_{sv} \quad (9) $$

$$ \mathbf{W}_2 = -\left[{}^{1b}\mathbf{p}_{2e}^{1e} \times \right] \cdot \mathbf{J}_{1\omega} + \mathbf{J}_{1v} \quad (10) $$

$$ \mathbf{W}_3 = \mathbf{J}_{2v} \quad (11) $$

${}^{A}\mathbf{p}_C^B$ is the vector that points from the origin of frame B to the origin of frame C expressed in frame A, ${}^{A}\mathbf{p}_C^B = {}^{A}\mathbf{R}_B\,{}^{B}\mathbf{p}_C$. $\left[{}^{A}\mathbf{p}_C^B \times \right]$ is the skew-symmetric matrix of the vector ${}^{A}\mathbf{p}_C^B$. The Jacobian matrices for the base stem are derived as:

$$ \mathbf{J}_{sv} = \begin{bmatrix} 0 & 0 \\ 0 & 0 \\ 0 & 1 \end{bmatrix}, \mathbf{J}_{s\omega} = \begin{bmatrix} 0 & 0 \\ 0 & 0 \\ 1 & 0 \end{bmatrix} \quad (12) $$

$\mathbf{J}_{1v}$, $\mathbf{J}_{1\omega}$, $\mathbf{J}_{2v}$ and $\mathbf{J}_{2\omega}$ are obtained from (4) and (5).

D. Optimization of the Manipulator Dimension

An optimization is conducted to improve the kinematic performance of the continuum manipulator.

1) Quantification of the Kinematic Performance

Generally, the kinematic performance of a manipulator is quantified by its translational and dexterous workspace. Since the translational workspace may not be directly affected by the dexterous workspace for a generic manipulator, it might be a dilemma to formulate a multi-objective optimization that properly balances the translational and dexterous workspace.

However, the position and orientation of the end effector of a continuum manipulator is usually coupled: the manipulator bends its segments to change the position of its end effector, and this would change the orientation of the end effector at the same time. Hence, the translational workspace can be highly affected to the dexterous workspace.

It was shown in previous studies [13, 14] that the kinematic performance is better for a continuum manipulator with bigger translational workspace: points on the boundary of the translational workspace usually involve the segments at their maximal or minimal bending, which leads to a limited capability for orienting the end effector. Using the size of the translational workspace to indicate the kinematic performance also reduces the computational power needed for evaluating the dexterous workspace, since the dexterous workspace may only be assessed by the Jacobian-based iterative inverse kinematics solution.

This paper hence follows the same approach to quantify the kinematic performance of the proposed continuum manipulator in Fig. 2(d).

The optimization objective is set to be the volume of the workspace above a transverse plane, as shown in Fig. 4. This volume is denoted as the 'effective volume', since the positions beneath the transverse plane are considered ineffective.

There is an unreachable cavity inside the translational workspace. And the transverse plane passes the top point of the unreachable cavity.

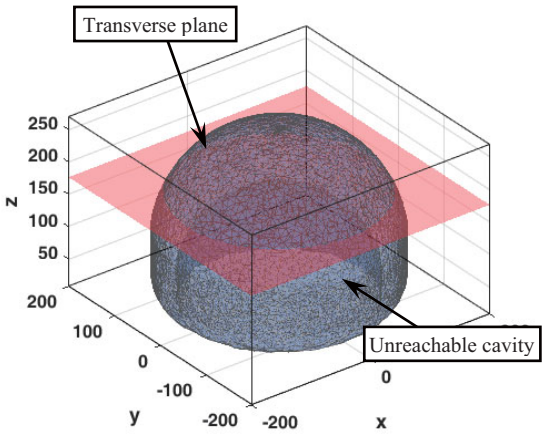

Figure 4. The manipulator workspace with a transverse plane.

2) Optimization and the Results

The optimization searches for the maximum of the effective volume by enumeration, since the effective volume has no analytical expression.

The effective volume of the workspace depends on the configuration variables of the manipulator ($\boldsymbol{\psi} = [\varphi\ d\ \theta_1\ \delta_1\ \theta_2\ \delta_2]^T$) if the structural variables (L_0, L_1, L_n and L_2) are given. L_0 indicates the translational range of the base stem: $d \in [0, L_0]$. And L_n is the length of the rigid segment.

The configuration variables have pre-defined ranges: $\theta_1 \in [0^o, 90^o]$, $\theta_2 \in [0^o, 120^o]$, $\delta_1 \in (-180^o, 180^o]$, and $\delta_2 \in (-180^o, 180^o]$.

The structural variables (L_0, L_1, L_n and L_2) are to be optimized. Constrained by the overall maximum length, the number of independent optimization variables is 3.

The ranges of the structural variables to be optimized are set based on the considerations as follows:

- Overall length $L_{sum} = L_0 + L_1 + L_n + L_2$ is set to 270 mm. This constraint introduces a realistic limit for surgical scenarios.
- The bending radius ρ_t of the t^{th} segment should be limited to a minimal value. The allowable strain is set at 1% for each individual backbone. The calculation of an individual backbone length can be found in [10]. In this paper, the bending radius $\rho_t \geq 80/\pi$ mm is set for all the continuum segments due to the consistent arrangement of the backbones in all segments. The bending radius constraints lead to the minimum length constraints for the continuum segments: $L_1 \geq 40$ mm and $L_2 \geq 60$ mm.

Then the following ranges for the structural variables to be optimized are used.

$$\begin{cases} 40 \leq L_1 \leq 80 \\ 0 \leq L_n \leq 60 \\ 60 \leq L_2 \leq 100 \end{cases} \tag{13}$$

The optimization was carried out by scanning the structural variables of L_1, L_n and L_2 in increments of 5 mm within their allowed ranges.

For a specific combination of the structural variables values, the translational workspace of the continuum manipulator is generated using the forward kinematics enumerating the configuration space $\boldsymbol{\psi} = [\varphi\ d\ \theta_1\ \delta_1\ \theta_2\ \delta_2]^T$.

Then the position of the transverse plane is located by searching the top point of the unreachable cavity in the workspace. The optimization objective values of each combination of the structural variables are visualized in Fig. 5(a).

From the results, the global optimum is achieved when $L_0 =$ 110 mm, $L_1 =$ 40 mm, $L_n =$ 25 mm, and $L_2 =$ 95 mm, with the corresponding value of the efficient volume being 6.065×10^6 mm^3.

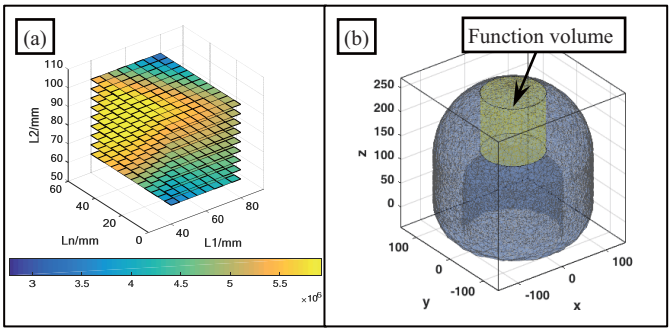

Figure 5. Optimization results: (a) the effective volumes with respect to the structural variables, (b) the workspace of the optimal structure with the function volumes enveloped.

3) Feasibility Check: Function Volume

Since the definition of the effective volume does not take the features during practical operation into consideration, a feasibility check was conducted to verify the validity of the optimal structure of the proposed surgical continuum manipulator.

Based on the estimation of the volumes of a few typical surgical sites, the function volume is defined to be a cylinder with a height of 120 mm and a diameter of 120 mm. The workspace of the manipulator should envelop the function volume completely.

As shown in Fig. 5(b), the required function volume is properly enveloped by the workspace of the optimized continuum manipulator. The optimal structure is verified to be feasible.

IV. Manipulator Motion Demonstration

The proposed continuum surgical manipulator design is implemented as standalone module in a surgical robotic system to show its performance. In this system, the continuum manipulator is controlled under teleoperation.

The continuum surgical manipulator module is shown in Fig. 6. It consists of i) the surgical tool, ii) the sterile barrier, and iii) the actuation unit.

- The actuation unit contains all motors and corresponding control units. It translates and rotates the surgical tool together with the sterile barrier, as well as generates several rotary outputs through the sterile barrier to drive proposed surgical manipulator at the distal end of the surgical tool.
- The sterile barrier is a physical isolation between the sterilized components and the unsterilized equipment. The sterile barrier transmits the driving motions from the actuation unit to the surgical tool, and transfers the signals from the surgical tool to the actuation unit.
- The surgical tool has the proposed surgical manipulator integrated at its distal end. It also contains the transmission chains that convert the motors' inputs into the push-pull driving motions for the segments' backbones in the continuum manipulator. During an operation, the surgical tool is mounted on the sterile barrier and its stem is inserted into a patient's abdominal to approach the surgical sites.

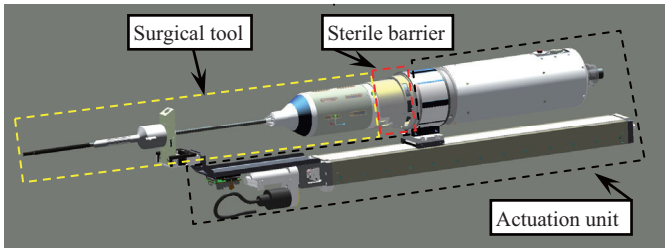

Figure 6. The propopsed continuum surgical manipulator module

In order to demonstrate the motion capability, a peg transfer experiment is carried out under the teleoperation control guided by a 3D laparoscope, as shown in Fig. 7.

The manipulator was able to carry out the transfer motions smoothly between the pegs. During the experiment, the rubber rings on one peg was transferred to another peg one by one. The operations that were performed in this process mainly included grasping, lifting, translating, and placing. No significant following error was observed during the operation. The optimized manipulator structure was then demonstrated to deliver satisfactory performances.

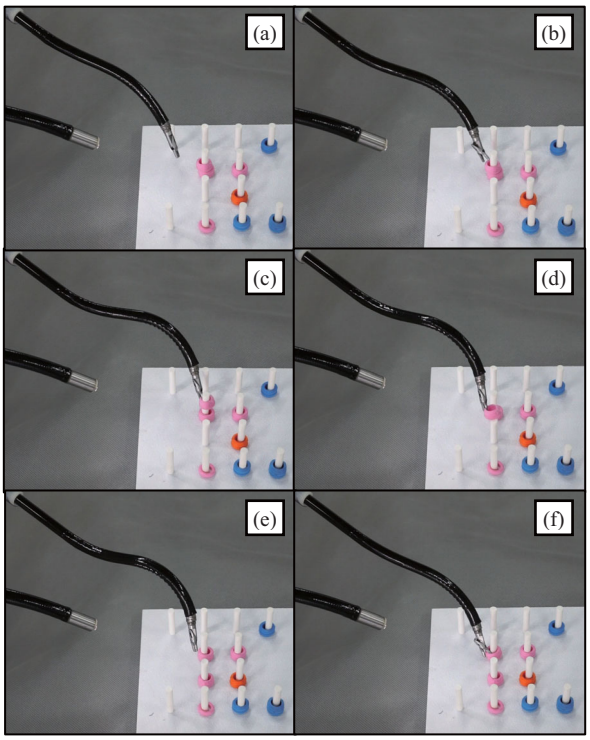

Figure 7. Preliminary validation experiment: the peg transfer task was accomplished with a teleoperation control under the guideance of a 3D laparoscope. Two sample rings were transferred to an adjacent peg with ease.

V. Conclusions and Future Works

Continuum surgical manipulators can potentially generate the required intra-abdominal movements without involving a RCM mechanism. However, their kinematics performances highly depend on their topologies and structural dimensions.

Due to the constraints stemmed from the actual implementation, a topology that was previously proved superior demonstrated limited kinematic performance. Hence this paper proposes an alternative topology and kinematic optimization of a 2-segment continuum surgical manipulator.

The optimization for the kinematic performance of the manipulator was conducted with a simplified objective. Such a strategy reduced the computational load for the optimization vastly. The enumeration optimization results provided an explicit view over the effects of each structural variable on the kinematic performance of the continuum manipulator. The results hence show insights to the kinematic features of the multi-segment continuum manipulator and provide inspirations for future topological synthesis.

The effectiveness of the proposed design was preliminarily validated in a surgical robotic system by performing a laparoscopic training task under teleoperation. The constructed manipulator would be extensively tested in the future experimental studies to fully demonstrate the efficacy of the proposed idea.

References

[1] R. H. Taylor, "A Perspective on Medical Robotics," *Proceedings of the IEEE,* vol. 94, No.9, pp. 1652- 1664, 2006.

[2] M. C. Cavusoglu, M. Cohn, F. Tendick, and S. Sastry, "A Laparoscopic Telesurgical Workstation," *IEEE Transactions on Robotics and Automation,* vol. 15, No.4, pp. 728-739, 1999.

[3] G. S. Guthart and J. K. Salisbury, "The Intuitive™ Telesurgery System: Overview and Application," in *IEEE International Conference on Robotics and Automation (ICRA)*, San Francisco, CA, 2000, pp. 618-621.

[4] P. Berkelman and J. Ma, "A Compact Modular Teleoperated Robotic System for Laparoscopic Surgery," *The International Journal of Robotics Research,* vol. 28, No.9, pp. 1198-1215, 2009.

[5] B. Hannaford, J. Rosen, D. W. Friedman, H. King, P. Roan, L. Cheng, D. Glozman, J. Ma, S. N. Kosari, and L. White, "Raven-II: An Open Platform for Surgical Robotics Research," *IEEE Transactions on Biomedical Engineering,* vol. 60, No.4, pp. 954-959, April 2013.

[6] C.-H. Kuo, J. S. Dai, and P. Dasgupta, "Kinematic Design Considerations for Minimally Invasive Surgical Robots: an Overview," *The International Journal of Medical Robotics and Computer Assisted Surgery,* vol. 8, No.2, pp. 127-145, June 2012.

[7] J. Burgner-Kahrs, D. C. Rucker, and H. Choset, "Continuum Robots for Medical Applications: A Survey," *IEEE Transactions on Robotics,* vol. 31, No.6, pp. 1261-1280, Dec 2015.

[8] K. Xu, R. E. Goldman, J. Ding, P. K. Allen, D. L. Fowler, and N. Simaan, "System Design of an Insertable Robotic Effector Platform for Single Port Access (SPA) Surgery," in *IEEE/RSJ International Conference on Intelligent Robots and Systems (IROS)*, St. Louis, MO, USA, 2009, pp. 5546-5552.

[9] S. Can, C. Staub, A. Knoll, A. Fiolka, A. Schneider, and H. Feussner, "Design, Development and Evaluation of a Highly Versatile Robot Platform for Minimally Invasive Single-Port Surgery," in *IEEE / RAS-EMBS International Conference on Biomedical Robotics and Biomechatronics (BIOROB)*, Roma, Italy, 2012, pp. 817-822.

[10] K. Xu, J. Zhao, and M. Fu, "Development of the SJTU Unfoldable Robotic System (SURS) for Single Port Laparoscopy," *IEEE/ASME Transactions on Mechatronics,* vol. 20, No.5, pp. 2133-2145, Oct 2015.

[11] J. Shang, K. Leibrandt, P. Giataganas, V. Vitiello, C. A. Seneci, P. Wisanuvej, J. Liu, G. Gras, J. Clark, A. Darzi, and G.-Z. Yang, "A Single-Port Robotic System for Transanal Microsurgery - Design and Validation," *IEEE Robotics and Automation Letters,* vol. 2, No.3, pp. 1510-1517, July 2017.

[12] J. Wang, S. Wang, J. Li, X. Ren, and R. M. Briggs, "Development of a Novel Robotic Platform with Controllable Stiffness Manipulation Arms for Laparoendoscopic Single-Site Surgery (LESS)," *The International Journal of Medical Robotics and Computer Assisted Surgery,* vol. EarlyView, p. e1838, 2017.

[13] K. Xu and X. Zheng, "Configuration Comparison for Surgical Robotic Systems Using a Single Access Port and Continuum Mechanisms," in *IEEE International Conference on Robotics and Automation (ICRA)*, Saint Paul, MN, USA, 2012, pp. 3367-3374.

[14] K. Xu, J. Zhao, and X. Zheng, "Configuration Comparison among Kinematically Optimized Continuum Manipulators for Robotic Surgeries through a Single Access Port," *Robotica,* vol. 33, No.10, pp. 2025-2044, Dec 2015.

[15] K. Xu and N. Simaan, "Intrinsic Wrench Estimation and Its Performance Index of Multi-Segment Continuum Robots," *IEEE Transactions on Robotics,* vol. 26, No.3, pp. 555-561, June 2010.

[16] R. J. Webster and B. A. Jones, "Design and Kinematic Modeling of Constant Curvature Continuum Robots: A Review " *International Journal of Robotics Research,* vol. 29, No.13, pp. 1661-1683, Nov 2010.

[17] K. Xu and N. Simaan, "Analytic Formulation for the Kinematics, Statics and Shape Restoration of Multibackbone Continuum Robots via Elliptic Integrals," *Journal of Mechanisms and Robotics,* vol. 2, No.011006, pp. 1-13, Feb 2010.